Nano Research

ISSN 1998-0124 CN 11-5974/O4
https://doi.org/10.1007/s12274-023-6275-9

Research Article

A Li_3P nanoparticle dispersion strengthened ultrathin Li metal electrode for high energy density rechargeable batteries

Lin Fu[1,2,§], Xiancheng Wang[2,§], Bao Zhang[3], Zihe Chen[2], Yuanjian Li[2,4], and Yongming Sun[2] (✉)

[1] *Provincial Guizhou Key Laboratory of Green Chemical and Clean Energy Technology, School of Chemistry and Chemical Engineering, Guizhou University, Guiyang 550025, China*
[2] *Wuhan National Laboratory for Optoelectronics, Huazhong University of Science and Technology, Wuhan 430074, China*
[3] *School of Physical and Mathematical Sciences, Nanyang Technological University, Singapore 637371, Singapore*
[4] *Institute of Materials Research and Engineering, Agency for Science Technology and Research (A*STAR), Singapore 138634, Singapore*
[§] *Lin Fu and Xiancheng Wang contributed equally to this work.*

Received: 9 August 2023 / **Revised:** 7 October 2023 / **Accepted:** 18 October 2023

ABSTRACT

Achievement of lithium (Li) metal anode with thin thickness (e.g., ≤ 30 μm) is highly desirable for rechargeable high energy density batteries. However, the fabrication and application of such thin Li metal foil electrode remain challenging due to the poor mechanical processibility and inferior electrochemical performance of metallic Li. Here, mechanico-chemical synthesis of robust ultrathin Li/Li_3P (LLP) composite foils (~ 15 μm) is demonstrated by employing repeated mechanical rolling/stacking operations using red P and metallic Li as raw materials. The *in-situ* formed Li^+-conductive Li_3P nanoparticles in metallic Li matrix and their tight bonding strengthen the mechanical durability and enable the successful fabrication of free-standing ultrathin Li metal composite foil. Besides, it also reduces the electrochemical Li nucleation barrier and homogenizes Li plating/stripping behavior. When matching to high-voltage $LiCoO_2$, the full cell with a low negative/positive (N/P) capacity ratio of ~ 1.5 offers a high energy density of ~ 522 $W{\cdot}h{\cdot}kg^{-1}$ at 0.5 C based on the mass of cathode and anode. Taking into account its facile manufacturing, potentially low cost, and good electrochemical performance, we believe that such an ultrathin composite Li metal foil design with nanoparticle-dispersion-strengthened mechanism may boost the development of high energy density Li metal batteries.

KEYWORDS

lithium metal anode, high energy density battery, mechanico-chemical synthesis, ultrathin Li/Li_3P composite foil, low negative/positive capacity ratio

1 Introduction

Lithium (Li) metal has been widely regarded as an ideal anode for rechargeable high energy density Li-based batteries due to its highest specific capacity (3860 $mA{\cdot}h{\cdot}g^{-1}$) and lowest electrochemical potential (−3.04 V vs. standard hydrogen electrode) among all the candidates [1, 2]. However, Li metal anode suffers from high reactivity and relatively large volume changes during the electrochemical stripping/plating cycling, which results in severe side reactions with electrolyte, heterogeneous Li stripping/plating behaviors, and eventually rapid electrochemical failure [3]. In the last few decades, numerous effective strategies, such as advanced electrolyte design, electrode interface engineering, and composite electrode fabrication, were extensively explored, which significantly enhanced the electrochemical performance of Li metal anodes [4, 5]. Unfortunately, most of the reported progresses were achieved based on the use of Li metal anode with large thickness (usually > 40 μm) [6, 7]. In consideration of practical application, introducing too much excess Li of thick Li metal anode not only increases the cost, but also significantly decreases the energy density of batteries [8]. To meet high energy demand of advanced rechargeable Li metal batteries with low negative/positive (N/P) capacity ratio (e.g., ≤ 2), the thickness of a reliable Li metal foil anode should be ≤ 40 μm in consideration of the areal capacity (e.g., 4 $mA{\cdot}h{\cdot}cm^{-2}$) of the state-of-art industrial cathodes [9, 10]. However, the poor mechanical processibility and stability of metallic Li make it very challenging to fabricate metallic Li foil with such thin thickness using conventional mechanical rolling approach in industry [11]. Vacuum evaporation is an effective approach for the fabrication of ultrathin metallic Li films with thickness less than 1 μm, but it is not feasible for the realization of metallic Li foils with suitable thickness from several micrometers to tens of several micrometers, which match the current cathodes [12]. Another challenge for practical ultrathin Li metal electrode is its poor electrochemical performance [13]. Due to the significantly reduced thickness, the failure mechanism of thin Li metal electrode becomes more complex than the thick counterpart, and the realization of stable electrochemical cycling is more challenging. Typically, a 50 μm-thick pure Li anode with the $LiCoO_2$ cathode of ~ 3 $mA{\cdot}h{\cdot}cm^{-2}$ often failed within 20 cycles in carbonate electrodes at 0.2 C [14]. Very recently, ultrathin Li/reduced graphene oxide (RGO) composite foils with thickness from 0.3 to 20 μm were fabricated through the absorption of molten metallic Li into the inner intervals of stacked RGO film

Address correspondence to yongmingsun@hust.edu.cn

and the Li/RGO electrode with thickness of 20 μm showed enhanced cycling stability than thin pure Li electrode, however, whose size was determined by the size and Li diffusion in planar dimension of RGO film [15]. Till now, exploration of scalable approaches for the fabrication of ultrathin Li metal foil electrodes with good electrochemical performance still remains a significant challenge.

Metal matrix composites are widely adopted to improve the mechanical durability of metals and withstand the forces for structural applications, which are highly dependent on the structure of composites, including the grain sizes of the matrix metal and solid dispersion, and the combination between them [16–18]. The solid dispersion provides additional reinforcement, prevents the grain boundary sliding and hinders the breakage/crack of the composites under rolling and/or bending external force [19, 20]. In principle, small size of solid dispersion material and its good binding/contact with the metal matrix are ideal for improving the mechanical processibility and stability, which helps to stabilize the grain boundary sliding and enhance the mechanical durability of materials, especially for soft metal materials like metallic Li [20–22].

Inspired by dispersion strengthened composite structure of metal matrix composites for structural applications, here we demonstrated a novel Li_3P dispersion strengthened ultrathin metallic Li composite foil, Li/Li_3P (LLP) foil, which was fabricated via the *in-situ* chemical reaction between metallic Li and red P by repeated mechanical rolling/stacking operations. Such a Li_3P dispersion strengthened LLP composite foil displayed the following characteristics: *in-situ* formed ultrafine Li_3P nanoparticles uniformly embedded into metallic Li matrix with low interfacial energy. The composite structure helped to withstand the external force for repeated rolling and bending, and resist the breakage/crack, and thus enabling the formation of mechanically robust free-standing ultrathin Li metal composite foils. Also, Li_3P in the LLP composite foil reduced the nucleation barrier for electrochemical Li plating, and extended the electrochemical cycle life [23, 24]. $LiCoO_2$||LLP full cell with 15 μm-thick LLP composite anode and N/P ratio of ~ 1.5 delivered high energy density of ~ 522 W·h·kg^{-1} at a current density of 0.5 C, as well as stable cycling. This work provides an alternative design for the fabrication of ultrathin Li-based composite foil electrode featured by dispersion strengthened structure, which brings hope to scalable manufacture of ultrathin Li metal electrode with low cost and superior electrochemical performance.

2 Experiment section

2.1 Materials synthesis and characterization

Ultrathin LLP composite foil was prepared via facile mechanical rolling/stacking operations under room temperature (Fig. S1 in the Electronic Supplementary Material (ESM)). Red P powder was uniformly placed between two pieces of pure Li foils to form a Li|P|Li sandwich and it converted to a compact hybrid foil after mechanical rolling under controlled pressure. The hybrid foil was then folded and stacked, which was followed by mechanical rolling for the second time. After many above-mentioned operations, a homogeneous LLP composite foil was obtained. Red P and metallic Li reacted to produce Li_3P during the processing. A composite foil featured that Li_3P nanoparticles uniformly embedded in the metallic Li matrix were finally formed after repeated rolling/stacking operations. The chemical composition characterizations were performed using X-ray diffraction (XRD, Empyrean) and X-ray photoelectron spectroscopy (XPS, AXIS-ULTRA DLD-600W). The morphology and microstructure information was collected using a field emission scanning electron microscopy (SEM, Gemini 300, Zeiss) equipped with an energy dispersive X-ray spectroscopy (EDS) analyzer (Oxford). The hardness details were achieved on Shore durometer (LX-A).

2.2 Computational method

The density functional theory (DFT) calculations were performed by using Vienna *ab-initio* simulation package (VASP) with projector augmented wave (PAW) method. The exchange-correlation energy was described by the functional of Perderw–Burke–Ernzerhof (PBE) form including van der Waals corrections (DFT-D3 method). The kinetic energy cutoff of electron wave functions was 520 eV. The geometry optimizations were performed by using the conjugated gradient method, and the convergence threshold was set to be 10^{-4} eV in energy and 0.02 eV·Å^{-1} in force. The Brillouin zone was sampled by using the Monkhorst–Pack scheme. The interfacial energy was evaluated using the same method in a previous work [25].

2.3 Electrochemical measurement

Coin cell (CR2032) assembly was carried out in an Ar-filled glove box, which employed Celgard 2500 polypropylene membrane as the separator. $LiFePO_4$ cathode with 97 wt.% active material was used as received (Shenzhen Kejing Star Technology Co. Ltd.) The $LiCoO_2$ cathode with 90 wt.% active material was prepared by a blade-casting method. 1 M bis(trifluoromethane)sulfonimide lithium salt (LiTSFI) in 1,2-dimethoxyethane (DME)/1,3-dioxolane (DOL) (1:1 by volume) with 2 wt.% $LiNO_3$ was used as the electrolyte for LLP||LLP, Li||Li, and $LiFePO_4$||LLP cells. The electrolyte for $LiCoO_2$||LLP full cells was 0.6 M $LiBF_4$ and 0.6 M lithium difluoro(oxalato)borate (LiDFOB) in diethyl carbonate (DEC)/fluorinated ethylene carbonate (FEC) (2:1 by volume). Linear sweep voltammetry (LSV) was performed in the voltage range of –0.13 to 0.13 V with a sweep rate of 0.1 mV·s^{-1} using a Biologic VMP3 workstation. Electrochemical impedance spectroscopy (EIS) of symmetric cells was measured in the frequency range of 100 kHz to 100 mHz with an alternating voltage amplitude of 10 mV on a Biologic VMP3 workstation. The polarization of symmetric cells was measured using above electrochemical workstation. Galvanostatic cycling was performed on a LAND battery tester (CT3001). The energy density for full cell was calculated based on the total mass of cathode and anode.

3 Results and discussion

The poor mechanical durability of metallic Li makes it easy to crack during mechanical rolling operation for the fabrication of ultrathin Li foils due to the unconfined dislocation movement upon deformation (Fig. S2 in the ESM) [7, 26]. Uniformly introducing particles in the metal matrix can effectively restrain the unconfined dislocation movement of metal matrix during rolling deformation and improve its mechanical durability, which is namely dispersion strengthening effect [21, 27]. Small particle size and uniform dispersion of nanoparticles within the matrix could enable good mechanical property of the composite, which require low interfacial energy between the particles and matrix [20]. The close contact between the nanoparticles and matrix, and good dispersion of nanoparticles into the Li matrix can effectively suppress the crack of composite during the mechanical rolling caused by the unconfined dislocation movement of metallic Li, thus improving its mechanical durability (Fig. 1) [21, 27].

Red P is soft and exists in a polymetric chain with network of phosphorus atoms (Fig. S3 in the ESM) [28]. Red P reacts with metallic Li mildly during the repeated rolling/stacking operations,

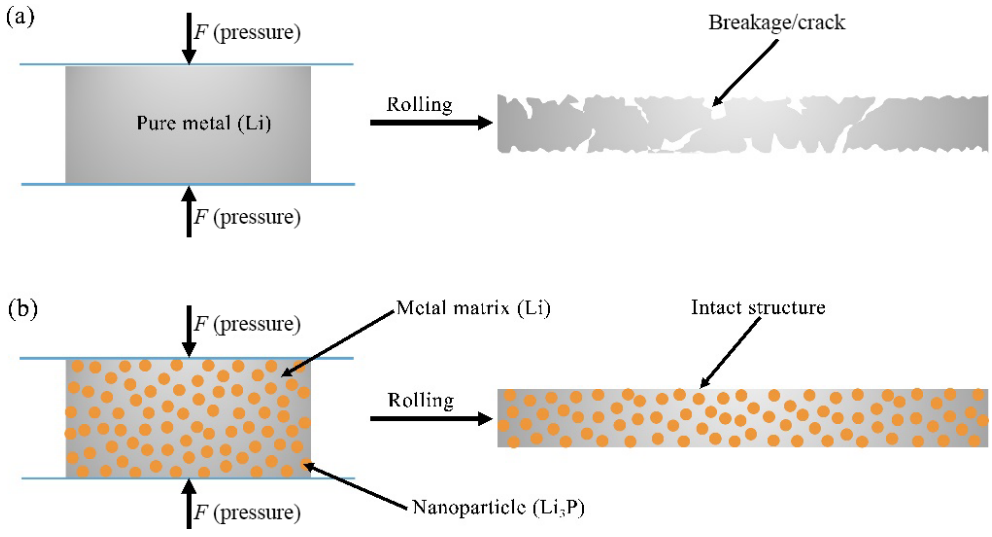

Figure 1 Schematic for the comparison of (a) pure Li foil and (b) LLP composite foil under external force.

which produces ultrafine Li_3P nanoparticles. Also, repeated mechanical rolling/stacking operations enable the dispersion of Li_3P into metallic Li matrix, which successfully improves the mechanism durability and processibility of metallic Li. To fabricate a mechanically robust ultrathin LLP composite foil, we revealed that the accurate control of the interval of the rolling machine for mechanical rolling/stacking operations made up a key step that enabled slow but complete conversion from red P to Li_3P as well as the well dispersion of Li_3P nanoparticles in the Li metal matrix. Using 20 wt.% red P and 80 wt.% metallic Li as the raw materials, ultrathin 15 μm-thick LLP composite foil was successfully fabricated. Benefiting from the composite structure of *in-situ* formed ultrafine Li_3P nanoparticles in the metallic Li matrix with low interfacial energy, the mechanical processability of LLP composite foil was significantly improved in comparison to pure Li foil. Note that the well-dispersed Li_3P with good ionic conductivity in the Li metal composite electrode could reduce the electrochemical Li nucleation potential, and enhance the reaction kinetics, thus improving the electrochemical performance of rechargeable Li metal batteries [23, 24]. Besides for promoting the Li^+ transport and reducing Li nucleation potential, Li_3P can also function as a robust skeleton to mitigate volume changes during Li plating/stripping processes.

The thermodynamic distribution of a material X in metallic Li can be quantified by its interfacial energy of X and Li. A lithiophilic material tends to be uniformly distributed in the bulk of metallic Li, while a lithiophobic material tends to be enriched on the surface or agglomerated [29]. In order to evaluate the lithiophilic/lithiophobic nature of Li_3P, we performed DFT calculations of the Li_3P (001)|Li (001) interface and calculated the interfacial energies. As shown in Fig. 2(a), the calculated surface energy of Li_3P (001) and Li (001) are about 0.73 and 0.56 $J{\cdot}m^{-2}$, respectively. The interfacial energy of Li_3P (001)|Li (001) is about 0.30 $J{\cdot}m^{-2}$ (Fig. 2(b)), indicating the lithiophilic nature of Li_3P. In this way, the Li_3P particles would be uniformly embedded into the Li bulk during mechanical rolling. The low interfacial energy between metallic Li and Li_3P, with the combination of continuous mechanical rolling/stacking operations, could inhibit the coarsening and agglomeration of the Li_3P dispersion material in the LLP composite. It could enhance the tensile and creep strength of composite, enabling good processing property [16, 19, 26]. Besides, the relationship between the interfacial energy of Li_3P (001)|Li (001) and number of metallic Li indicates that the content of Li_3P is a key parameter for the successful fabrication of ultrathin LLP composite foil (Fig. 2(c)).

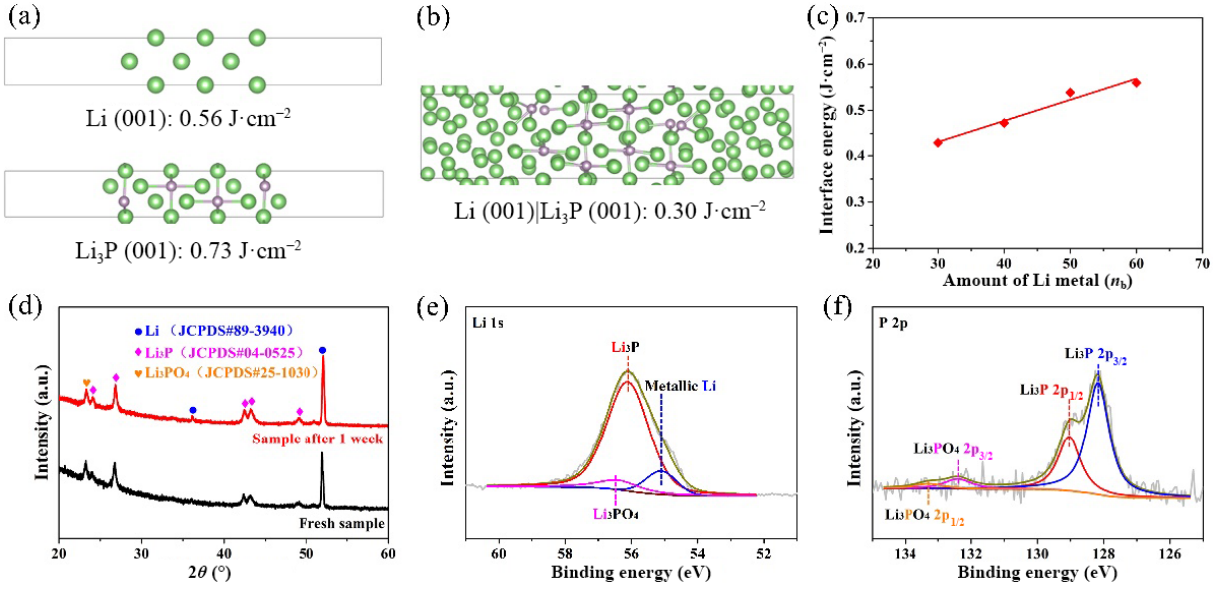

Figure 2 (a) Surface energies of Li_3P (001) and Li (001). (b) Interfacial energy of Li_3P (001)|Li (001). (c) Plots of the interfacial energy of Li_3P (001)|Li (001) and amount of Li metal. (d) XRD patterns of the LLP composite foil before and after resting in Ar atmosphere for 1 week. High-resolution (e) Li 1s and (f) P 2p XPS spectra of the LLP composite foil.

Based on the consideration of tradeoff between processibility and electrochemical performance (Fig. S4(a) in the ESM), LLP composite foil with 20 wt.% red P was selected as a model example for further investigation. Moreover, the nucleation overpotential gradually decreases with the increase of Li_3P content (Fig. S4(b) in the ESM), which could be attributed to the lithiophilic nature of Li_3P [30]. Its phase information was analyzed by XRD patterns. As shown in Fig. 2(d), the LLP composite mainly consisted of hybrid phases of metallic Li (JCPDS#89-3940) and Li_3P (JCPDS#04-0525). The weak diffraction peak at 23° suggested the existence of Li_3PO_4 (JCPDS#25-1030) produced by the reaction between metallic Li and oxides on the surface of the initial red P raw material. Moreover, the XRD pattern remained unchanged after resting for 1 week in comparison with the fresh counterpart, which suggested the good stability of LLP composite foil. XPS was carried out to detect the chemical composition information of the LLP composite foil. The deconvolutions of broad peaks were carefully assigned to the specific peaks that reflected the various element states. As shown in Fig. 2(e), the high-resolution Li 1s spectrum contained three characteristic peaks for metallic Li (55.1 eV), Li_3P (56.1 eV), and Li_3PO_4 (56.4 eV) [31–33]. The binding energy of metallic Li in the LLP is consistent with the pure Li (Fig. S5 in the ESM). The high-resolution P 2p spectrum displayed a pair of peaks at 128.17 and 129.04 eV, which corresponded to the orbitals of P $2p_{3/2}$ and P $2p_{1/2}$ in Li_3P, respectively (Fig. 2(f)) [33, 34]. Besides, a pair of weak peaks at 132.4 and 133.27 eV could be attributed to the signals of P $2p_{3/2}$ and P $2p_{1/2}$ from the surficial Li_3PO_4 in the composite, respectively [24, 34]. The above XPS results verified the main constituents of metallic Li and Li_3P for LLP foil, in agreement with the XRD results.

SEM was employed for morphology and microstructure investigations of LLP composite foil. LLP composite foil presented a smooth surface (Fig. 3(a)), while obvious indentation was observed for the pure Li foil (Fig. S6 in the ESM). Such a phenomenon indicated that the introduction of Li_3P caused the enhanced processibility and mechanical stability of metallic Li, beneficial for fabrication of high-quality foil electrode. The result of cross-section SEM image in Fig. 3(b) verified the dense structure of LLP composite foil, and thus the close contact between Li_3P and metallic Li without intervals or voids due to their low interfacial energy. The corresponding EDS mapping images indicated that P element was uniformly distributed over the LLP composite foil, suggesting the uniform embedment of *in-situ* formed Li_3P nanoparticles in the metallic Li matrix and no residual red P powders with large size (Fig. 3(b) and Fig. S7 in the ESM). Since the delithiation of Li_3P occurred above 0.75 V (vs. Li^+/Li), metallic Li in the LLP composite electrode could be fully stripped with the cut-off voltage of 0.5 V (vs. Li^+/Li), under which Li_3P remained unchanged [35, 36]. The average size of Li_3P particles was about 390 nm based on SEM investigation for LLP composite electrode after metallic Li stripping (Fig. 3(c)). Such small size of Li_3P nanoparticles and their uniform embedment in metallic Li with close contact are crucial factors in enhancing the processibility and successful fabrication of free-standing ultrathin Li-based composite foil. The poor mechanical processability of pure metallic Li foil encounters frequently breakage/crack owing to the unconfined dislocation movement during large plastic deformation operations [26]. Also, pure metallic Li foil tends to adhere on the surface of roller during the mechanical rolling due to its sticky nature, which aggravates the breakage/crack of foil structure [13]. Figure 3(d) shows the Shore hardness values of LLP composite and pure Li foils, respectively. The hardness value for LLP composite foil was up to ~ 89.5 hardness of aluminum (HA), which was much higher than that of pure Li foil (~ 72.1 HA). This result indicated that Li_3P nanoparticles efficiently enhanced the mechanical strength of metallic Li due to the dispersion strengthening effort on suppressing the breakage/crack of Li foil during the rolling process [13]. A schematic illustration on the viscosity investigation of the LLP composite and pure Li foils is

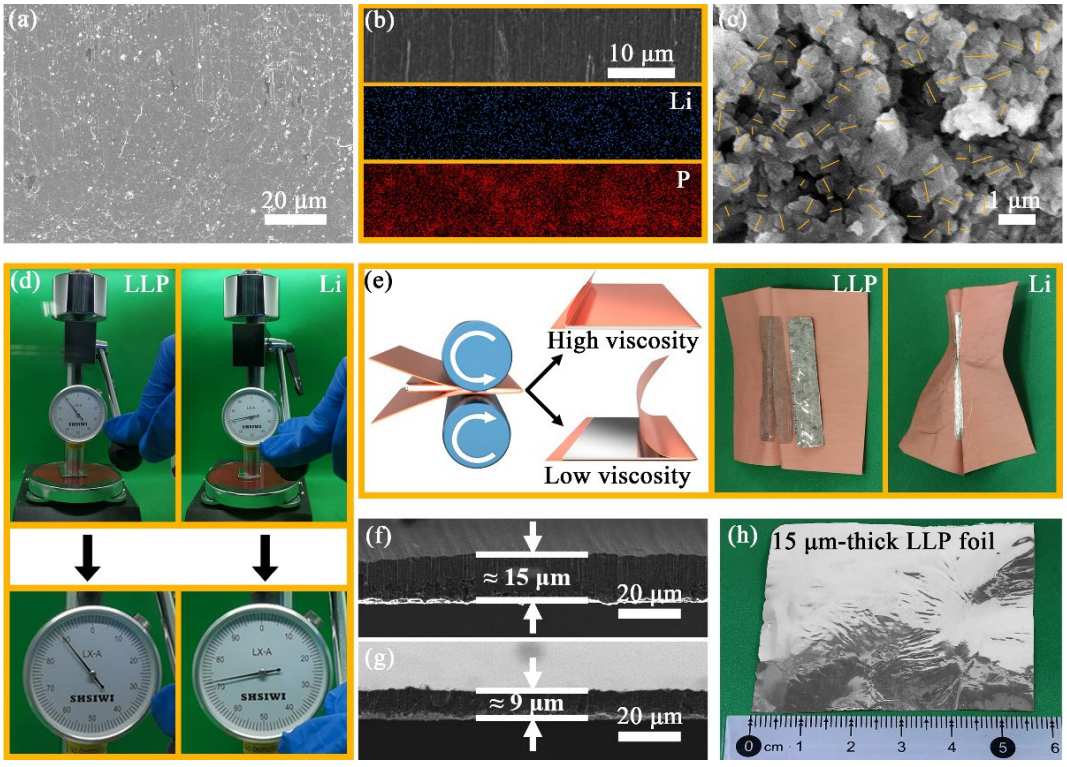

Figure 3 (a) Top-view SEM image and (b) cross-section SEM image of LLP composite foil and the corresponding EDS mapping images. (c) SEM image of LLP composite electrode after electrochemical Li stripping with cut-off voltage of 0.5 V (vs. Li^+/Li). (d) Digital photos of hardness measurement for LLP composite and pure Li foils. (e) Schematic for viscosity test and digital photos of LLP composite and pure Li foils after the test. ((f) and (g)) Cross-section SEM images of LLP composite foils with different thicknesses. (h) Digital photo of 15 μm-thick LLP composite foil.

shown in Fig. 3(e). The sample was placed between two pieces of Cu foils and pressed closely to form a sandwich structure by mechanical rolling operation under pressure of 3 MPa. Due to the high viscosity of pure metallic Li, it was glued to the Cu foils tightly and couldn't be separated easily. Larger strain could damage the pure Li foil but not enable the complete separation for the Cu and pure Li foils. In contrast, the LLP composite foil was easily peeled off and intact foil morphology was maintained after its separation with the Cu foils, indicating the weak adhesiveness between them. Such an enhanced mechanical property of LLP composite foil with significantly increased hardness and decreased viscosity could be explained by the dispersion strengthening effect with uniformly dispersed Li_3P nanoparticles in metallic Li matrix. As expected, a free-standing LLP composite foil with thickness < 30 μm was easily realized by mechanical rolling operation (Fig. 3(f) and Fig. S8 in the ESM). For example, a piece of ~ 15 μm-thick LLP composite foil with a width of 4 cm and a length of 5.5 cm was fabricated in our lab (Fig. 3(h)), which could be even thinner for samples with smaller size (e.g., ~ 9 μm, 2.5 cm × 4.5 cm, Fig. 3(g) and Fig. S9 in the ESM). It is noted a higher P proportion of 30 wt.% displayed inferior mechanical ductility in comparison to LLP with 20 wt.% P. Too high P proportion would cause its incomplete reaction with metallic Li, and the residual red P powders and superabundant Li_3P could lead to brittle mechanical property of the LLP composite (Fig. S10 in the ESM). Dispersion strengthening for enhancing the processibility of soft and sticky metallic Li is potentially scalable and low cost, and is thus promising for the industrial fabrication of thin Li metal foils. Based on the above result and discussion, we believe that this method can be used to fabricate other ultrathin alkali metal composite foils with enhanced mechanical property and electrochemical performance.

The morphological evolution for LLP and pure Li electrodes was investigated using SEM. Although similar granular Li deposits with large grain size (up to 10 μm) were observed for both the LLP composite and pure Li electrodes after initial Li plating (Figs. S11(a) and S11(b) in the ESM), they showed quite different morphology after Li stripping. The LLP composite electrode displayed smooth surface after initial Li stripping (Fig. S11(c) in the ESM), while pure Li showed obvious pits on the electrode surface (Fig. S11(d) in the ESM). Importantly, the LLP composite electrode could maintain its initial intact morphology after repeated Li plating/stripping cycling (50 cycles, Fig. S12(a) in the ESM). In contrast, the cycled pure Li electrode presented a nonuniform and porous surface (Fig. S12(b) in the ESM). The above results indicated that the introduction of Li_3P could homogenize electrochemical reaction and inhibit the irreversible consumption of active Li.

To explore the effect of Li_3P for electrochemical performance, XPS analysis was conducted after Ar-ion etching of 5 min for the LLP composite and pure Li electrodes after 50 cycles. The peak at 56.1 eV in the high-resolution Li 1s spectrum (Fig. 4(a)) and the peaks at 128.17 and 129.04 eV in the high-resolution P 2p spectrum (Fig. 4(b)) verified the existence of Li_3P in the cycled LLP composite [33, 34]. However, the areal proportion of these peaks to others obviously decreased in comparison to the case of the fresh LLP composite foil. Moreover, characteristic peak pair at 132.4 and 133.27 eV showed significantly enhanced intensity for the cycled LLP composite in comparison to that for the fresh LLP composite, which related to the orbitals of P $2p_{3/2}$ and P $2p_{1/2}$ of Li_3PO_4, respectively [24, 34]. Besides, the LLP composite anode showed a weak peak at 56.1 eV and a strong peak at 56.4 eV in the high-resolution Li spectrum, which were attributed to the signals of Li_3P and Li_3PO_4/Li_2CO_3, respectively [32, 33, 37]. These results suggested that partial Li_3P converted to Li_3PO_4 on electrode surface via the reaction between Li_3P and electrolyte. Note that Li_3PO_4 is a superior interfacial stabilizer for Li metal anode [38, 39]. The Li_3PO_4 and Li_3P with high ionic conductivity participated in the formation of solid electrolyte interphase (SEI), which could help to extend the electrochemical cycling life of batteries [34, 38]. Both the cycled LLP composite and pure Li electrodes displayed a characteristic peak at 55.1 eV for metallic Li in high-resolution Li 1s spectra (Figs. 4(a) and 4(c), and Fig. S5 in the ESM) [31]. The peaks at 55.3, 55.7, and 57.2 eV could be ascribed to Li_2O, $ROCO_2Li$ (R refers to organic functional group), and LiF resulted from the reaction products between the electrode and electrolyte, respectively, which were also the components of the SEI on the electrode [40–42]. The stable SEI can effectively suppress irreversible consumption of active Li and prolong the cycle life of battery (Figs. 4(d) and 4(e)). As shown in Fig. 4(f), the exchange current density of LLP composite is 0.1644 $mA·cm^{-2}$, which is much higher than 0.0644 $mA·cm^{-2}$ for the pure Li. The increase in exchange current density of the LLP composite indicates the enhanced charge transfer at the electrode/electrolyte interface [11]. The Li^+ transference number (t_{Li^+}) was used to further reveal the advantage of the LLP/electrolyte interface over the pure Li/electrolyte, which was obtained by the potentiostatic polarization method [43]. The t_{Li^+} increased from 0.236 for the pure Li to 0.355 for the LLP composite, which was attributed to that the LLP could be interacted with the Li salt to increase the ion pair (Li^+ and $TSFI^-$) dissociation and enhance the fraction of free Li^+ (Figs. 4(g)–4(i) and Table S1 in the ESM) [43, 44]. This result demonstrates the positive effect of Li_3P in the LLP composite on enhancing Li^+ diffusion via its interaction with electrolyte on electrode surface. Therefore, introduction of Li_3P in LLP composite can improve the reaction kinetics of electrode/electrolyte and enhance the electrochemical performance of rechargeable Li metal batteries.

To evaluate electrochemical performances of the as-prepared ultrathin Li composite foils, symmetric and full cells were assembled and tested. The Coulombic efficiency (CE) of the LLP composite electrode was further evaluated according to the previous publications (Fig. S13 in the ESM) [45, 46]. The average CE (ACE) of LLP composite reached as high as 99.6% for 25 Li plating/stripping cycles at 1 $mA·cm^{-2}$ and 1 $mA·h·cm^{-2}$, which was significantly higher than that of pure Li (98.7%, Fig. S14 in the ESM). These results indicated that presence of Li_3P could restrain side reactions between the metallic Li and electrolyte, and reduce irreversible consumption of active Li, which was consistent with results of the SEM investigation (Figs. 4(d) and 4(e)).

The symmetrical cell with 30 μm-thick LLP composite electrode displayed a long cycle lifespan of 500 h with a low and constant overpotential of ~ 15 mV under a current density of 1 $mA·cm^{-2}$ and a fixed capacity of 1 $mA·h·cm^{-2}$ (Fig. 5(a)). Using the 15 μm-thick LLP foil electrode, the symmetrical cell survived over 300 h with similar voltage profiles under the same test conditions. Such good cycling stability could be explained by the reduced Li nucleation barrier and increased the conductivity of electrode due to the introduced Li_3P nanoparticles within metallic Li matrix [23]. As shown in Fig. 5(b) and Fig. S15 in the ESM, a reasonable area capacity of ~ 2.1 $mA·h·cm^{-2}$ and a high gravimetric specific capacity of ~ 2405 $mA·h·g^{-1}$ could be extracted by a 15 μm-thick foil under a cut-off voltage of 0.5 V, suggesting the high active Li utilization of LLP composite electrode. In order to demonstrate the potential application of LLP composite anode in rechargeable high energy density batteries, commercial $LiFePO_4$ cathodes were used to pair with thin LLP foil anodes for full cells (Fig. S16 in the ESM). With a low N/P ratio of ~ 2.0, $LiFePO_4$||LLP full cell with 30 μm-thick LLP anode sustained stable cycling for 100 cycles with negligible capacity decay under a current density of 1 C (1 C =

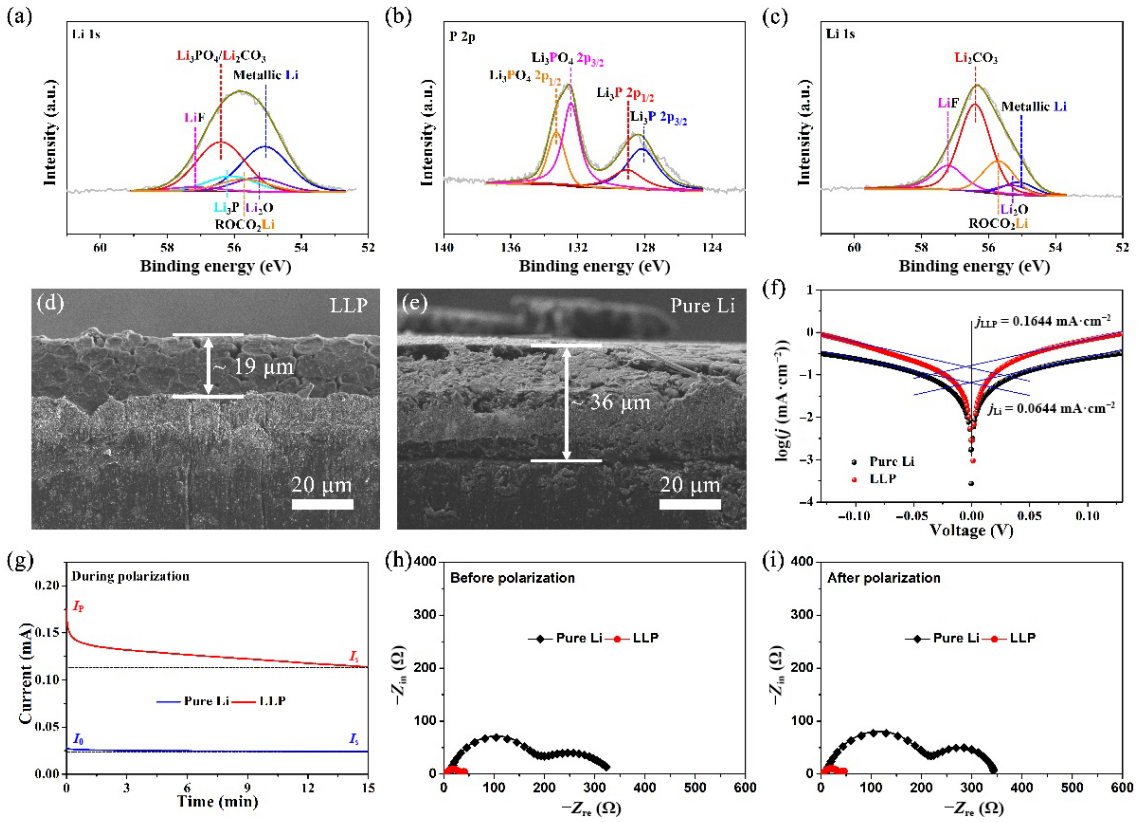

Figure 4 High-resolution (a) Li 1s and (b) P 2p XPS spectra of the LLP foil after 50 cycles. (c) High-resolution Li 1s XPS spectrum of the pure Li foil after 50 cycles. Cross-sectional SEM images of the (d) LLP and (e) pure Li electrodes after 50 cycles. The samples for (a)–(e) were obtained from Li||Li and LLP||LLP symmetric cells after cycling under a current density of 1 mA·cm^{-2} and a fixed capacity of 1 mA·h·cm^{-2}. (f) Tafel curves of Li||Li and LLP||LLP symmetric cells derived from LSV tests. (g) Chronoamperometry results of t_{Li^+} for the LLP and pure Li electrodes at 10 mV polarization. Nyquist plots (h) before and (i) after polarization of Li||Li and LLP||LLP symmetric cells.

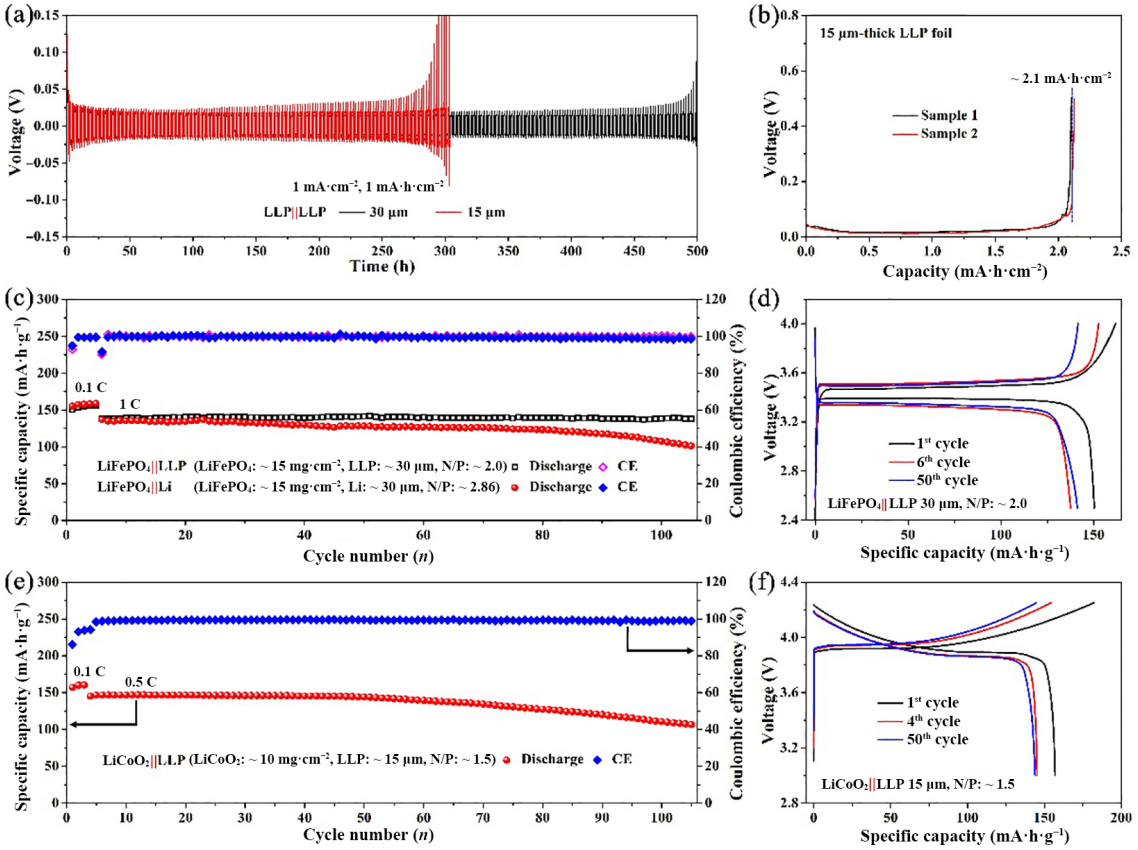

Figure 5 (a) Galvanostatic voltage–time curves of LLP||LLP cells with 30/15 μm-thick LLP electrodes. (b) Electrochemical delithiation curves of 15 μm-thick LLP foil electrodes. (c) Cycling performance of the $LiFePO_4$||LLP and $LiFePO_4$||Li full cells with 30 μm-thick LLP/pure Li anodes and (d) the corresponding voltage–capacity curves at 0.1 C (the initial five cycles) and 1 C (the following cycles). (e) Cycling performance of the $LiCoO_2$||LLP full cell with 15 μm-thick LLP anode and $LiCoO_2$ cathode and (f) the corresponding voltage–capacity curves at 0.1 C (the initial three cycles) and 0.5 C (the following cycles).

150 mA·g^{-1}, Fig. 5(c)), which far outperformed the counterpart with 30 μm-thick pure Li anode. As shown in Fig. S17 in the ESM, 30 μm-thick LLP anode was used to assemble $LiCoO_2$||LLP full cell. It exhibited favorable cycling performance with capacity retention of 83.1% for 100 cycles under a current density of 0.5 C (1 C = 140 mA·g^{-1}). As a contrast, the counterpart with 30 μm-thick pure Li anode displayed stable cycling for only ~ 30 cycles, and its capacity quickly decayed to 35.9% for 100 cycles. These results demonstrate that the introduction of Li_3P significantly improves the electrochemical performance of Li metal anode in full cell configuration. To further explore the practicability of the as-fabricated LLP composite anode, $LiCoO_2$||LLP full cell was fabricated with 15 μm-thick LLP composite anode and low N/P ratio of ~ 1.5, and it demonstrated stable cycling for 70 cycles at a current density of 0.5 C between 3 and 4.25 V (Fig. 5(e)), delivering a high energy density of ~ 522 W·h·kg^{-1} based on the total mass of cathode and anode. It should be pointed out that the electrochemical cycling stability of full cells could be further improved by employing advanced electrolytes [47]. In addition, $LiFePO_4$||LLP and $LiCoO_2$||LLP full cells showed stable voltage–capacity curves on cycling in comparison to their counterparts with pure Li metal foil, demonstrating that introduction of Li_3P in metallic Li would not cause any negative effects on electrochemical charge/discharge behavior (Figs. 5(d) and 5(f), and Fig. S18 in the ESM).

4 Conclusion

In summary, we propose a facile strategy for the fabrication of ultrathin Li metal composite foil with dispersion strengthening mechanism. Li_3P nanoparticles produced by *in-situ* mechanico-chemical reaction between red P and metallic Li improved mechanical durability of metallic Li foil, suppressed its breakage/crack under external force, and enabled the successful fabrication of ultrathin LLP composite with thickness less than 30 μm by facile mechanical rolling/stacking operations. Furthermore, functional component of Li_3P also helped to reduce the electrochemical Li nucleation barrier and increase the ionic conductivity of the electrode, which were beneficial for achieving good electrochemical properties. $LiFePO_4$||LLP full cell with 30 μm-thick LLP composite anode and N/P ratio of ~ 2.0 exhibited stable cycling for 100 cycles with negligible capacity decay at 1 C. $LiCoO_2$||LLP full cell with 15 μm-thick LLP composite anode and N/P ratio of ~ 1.5 displayed high energy density of ~ 522 W·h·kg^{-1} at 0.5 C. The facile fabrication, good mechanical processability and stable electrochemical performance of ultrathin LLP composite foil, as well as potential low cost, provide great potential for its practical application in rechargeable high energy density Li metal batteries.

Acknowledgements

Y. S. acknowledges the financial support by National Natural Science Foundation of China (No. 52272207). L. F. thanks the financial support by National Natural Science Foundation of China (No. 22209031), Guizhou Provincial Basic Research Program (Natural Science) (No. QKHJC-ZK[2023]YB046), and Natural Science Special Foundation of Guizhou University (No. X2022122 Special Post B).

Electronic Supplementary Material: Supplementary material (all experimental data and detailed procedures) is available in the online version of this article at https://doi.org/10.1007/s12274-023-6275-9.

References

[1] Cheng, X. B.; Zhang, R.; Zhao, C. Z.; Zhang, Q. Toward safe lithium metal anode in rechargeable batteries: A review. *Chem. Rev.* **2017**, *117*, 10403–10473.

[2] Peng, K. Y.; Tang, P.; Yao, Q. Q.; Dou, Q. Y.; Yan, X. B. Bifunctional fluoropyridinium-based cationic electrolyte additive for dendrite-free Li metal anode. *Nano Res.* **2023**, *16*, 9530–9537.

[3] Lin, D. C.; Liu, Y. Y.; Cui, Y. Reviving the lithium metal anode for high-energy batteries. *Nat. Nanotechnol.* **2017**, *12*, 194–206.

[4] Liu, D. H.; Bai, Z. Y.; Li, M.; Yu, A. P.; Luo, D.; Liu, W. W.; Yang, L.; Lu, J.; Amine, K.; Chen, Z. W. Developing high safety Li-metal anodes for future high-energy Li-metal batteries: Strategies and perspectives. *Chem. Soc. Rev.* **2020**, *49*, 5407–5445.

[5] Hao, Z. M.; Li, G.; Lu, Y.; Cai, Y. C.; Yang, G. J.; Chen, J. Anion-derived solid electrolyte interphase realized in usual-concentration electrolyte for Li metal batteries. *Nano Res.* **2023**, *16*, 12647–12654.

[6] Zhang, X. Q.; Li, T.; Li, B. Q.; Zhang, R.; Shi, P.; Yan, C.; Huang, J. Q.; Zhang, Q. A sustainable solid electrolyte interphase for high-energy-density lithium metal batteries under practical conditions. *Angew. Chem., Int. Ed.* **2020**, *59*, 3252–3257.

[7] Hu, M. T.; Tong, Z. M.; Cui, C.; Zhai, T. Y.; Li, H. Q. Facile, atom-economic, chemical thinning strategy for ultrathin lithium foils. *Nano Lett.* **2022**, *22*, 3047–3053.

[8] Gao, J. L.; Chen, C. J.; Dong, Q.; Dai, J. Q.; Yao, Y. G.; Li, T. Y.; Rundlett, A.; Wang, R. L.; Wang, C. W.; Hu, L. B. Stamping flexible Li alloy anodes. *Adv. Mater.* **2021**, *33*, 2005305.

[9] Zhan, Y. X.; Shi, P.; Ma, X. X.; Jin, C. B.; Zhang, Q. K.; Yang, S. J.; Li, B. Q.; Zhang, X. Q.; Huang, J. Q. Failure mechanism of lithiophilic sites in composite lithium metal anode under practical conditions. *Adv. Energy Mater.* **2022**, *12*, 2103291.

[10] Niu, C. J.; Lee, H.; Chen, S. R.; Li, Q. Y.; Du, J.; Xu, W.; Zhang, J. G.; Whittingham, M. S.; Xiao, J.; Liu, J. High-energy lithium metal pouch cells with limited anode swelling and long stable cycles. *Nat. Energy* **2019**, *4*, 551–559.

[11] Du, J. M.; Wang, W. Y.; Wan, M. T.; Wang, X. C.; Li, G. C.; Tan, Y. C.; Li, C. H.; Tu, S. B.; Sun, Y. M. Doctor-blade casting fabrication of ultrathin Li metal electrode for high-energy-density batteries. *Adv. Energy Mater.* **2021**, *11*, 2102259.

[12] Kato, A.; Hayashi, A.; Tatsumisago, M. Enhancing utilization of lithium metal electrodes in all-solid-state batteries by interface modification with gold thin films. *J. Power Sources* **2016**, *309*, 27–32.

[13] Zhang, C.; Fan, H. M.; Chen, X. L.; Xu, H.; Lou, J. T.; Li, Y.; Huang, Y. H.; Li, S. Non-sticky Li-alloy leaves for long-lasting secondary batteries. *Energy Environ. Sci.* **2022**, *15*, 5251–5260.

[14] Fu, L.; Wan, M. T.; Zhang, B.; Yuan, Y. F.; Jin, Y.; Wang, W. Y.; Wang, X. C.; Li, Y. J.; Wang, L.; Jiang, J. J. et al. A lithium metal anode surviving battery cycling above 200 °C. *Adv. Mater.* **2020**, *32*, 2000952.

[15] Chen, H.; Yang, Y. F.; Boyle, D. T.; Jeong, Y. K.; Xu, R.; De Vasconcelos, L. S.; Huang, Z. L.; Wang, H. S.; Wang, H. X.; Huang, W. X. et al. Free-standing ultrathin lithium metal-graphene oxide host foils with controllable thickness for lithium batteries. *Nat. Energy* **2021**, *6*, 790–798.

[16] Xu, B. B.; Guo, F. L. Upper and lower bounds on the creep strain and stress relaxation induced by interface diffusion in metal-matrix particulate composites. *Int. J. Solids Struct.* **2021**, *216*, 222–230.

[17] Ghodrati, H.; Ghomashchi, R. Effect of graphene dispersion and interfacial bonding on the mechanical properties of metal matrix composites: An overview. *FlatChem* **2019**, *16*, 100113.

[18] Alaneme, K. K.; Okotete, E. A.; Fajemisin, A. V.; Bodunrin, M. O. Applicability of metallic reinforcements for mechanical performance enhancement in metal matrix composites: A review. *Arab J. Basic Appl. Sci.* **2019**, *26*, 311–330.

[19] Paknia, A.; Pramanik, A.; Dixit, A. R.; Chattopadhyaya, S. Effect of size, content and shape of reinforcements on the behavior of metal matrix composites (MMCs) under tension. *J. Mater. Eng. Perform.* **2016**, *25*, 4444–4459.

[20] Liu, Q.; Qi, F. G.; Wang, Q.; Ding, H. M.; Chu, K. Y.; Liu, Y.; Li, C. The influence of particles size and its distribution on the degree of

stress concentration in particulate reinforced metal matrix composites. *Mater. Sci. Eng. A* **2018**, *731*, 351–359.
[21] Tjong, S. C. Novel nanoparticle-reinforced metal matrix composites with enhanced mechanical properties. *Adv. Eng. Mater.* **2007**, *9*, 639–652.
[22] Yang, H.; Jiang, L.; Balog, M.; Krizik, P.; Schoenung, J. M. Reinforcement size dependence of load bearing capacity in ultrafine-grained metal matrix composites. *Metall. Mater. Trans. A* **2017**, *48*, 4385–4392.
[23] Yu, W.; Yang, J.; Li, J. L.; Zhang, K.; Xu, H. M.; Zhou, X.; Chen, W.; Loh, K. P. Facile production of phosphorene nanoribbons towards application in lithium metal battery. *Adv. Mater.* **2021**, *33*, e2102083.
[24] Kim, Y.; Koo, D.; Ha, S.; Jung, S. C.; Yim, T.; Kim, H.; Oh, S. K.; Kim, D. M.; Choi, A.; Kang, Y. Y. et al. Two-dimensional phosphorene-derived protective layers on a lithium metal anode for lithium-oxygen batteries. *ACS Nano* **2018**, *12*, 4419–4430.
[25] Fan, X. L.; Ji, X.; Han, F. D.; Yue, J.; Chen, J.; Chen, L.; Deng, T.; Jiang, J. J.; Wang, C. S. Fluorinated solid electrolyte interphase enables highly reversible solid-state Li metal battery. *Sci. Adv.* **2018**, *4*, eaau9245.
[26] Xu, C.; Ahmad, Z.; Aryanfar, A.; Viswanathan, V.; Greer, J. R. Enhanced strength and temperature dependence of mechanical properties of Li at small scales and its implications for Li metal anodes. *Proc. Natl. Acad. Sci. USA* **2017**, *114*, 57–61.
[27] Li, S. J.; Wei, B. W.; Xu, J. J.; Xu, G. M.; Li, Y.; Wang, Z. D. High solid–solution strengthening mechanism of a novel aluminum-lithium alloy fabricated by electromagnetic near-net shape technology. *Mater. Sci. Eng. A* **2022**, *829*, 142148.
[28] Zhang, S.; Qian, H. J.; Liu, Z. H.; Ju, H. Y.; Lu, Z. Y.; Zhang, H. M.; Chi, L. F.; Cui, S. X. Towards unveiling the exact molecular structure of amorphous red phosphorus by single-molecule studies. *Angew. Chem., Int. Ed.* **2019**, *58*, 1659–1663.
[29] Wang, T. R.; Duan, J.; Zhang, B.; Luo, W.; Ji, X.; Xu, H. H.; Huang, Y.; Huang, L. Q.; Song, Z. Y.; Wen, J. Y. et al. A self-regulated gradient interphase for dendrite-free solid-state Li batteries. *Energy Environ. Sci.* **2022**, *15*, 1325–1333.
[30] Wood, K. N.; Kazyak, E.; Chadwick, A. F.; Chen, K. H.; Zhang, J. G.; Thornton, K.; Dasgupta, N. P. Dendrites and pits: Untangling the complex behavior of lithium metal anodes through *operando* video microscopy. *ACS Cent. Sci.* **2016**, *2*, 790–801.
[31] Zhao, Q.; Hao, X. G.; Su, S. M.; Ma, J. B.; Hu, Y.; Liu, Y.; Kang, F. Y.; He, Y. B. Expanded-graphite embedded in lithium metal as dendrite-free anode of lithium metal batteries. *J. Mater. Chem. A* **2019**, *7*, 15871–15879.
[32] Zhu, P. F.; Jiang, Z. P.; Sun, W.; Yang, Y.; Silvester, D. S.; Hou, H. S.; Banks, C. E.; Hu, J. G.; Ji, X. B. Built-in anionic equilibrium for atom-economic recycling of spent lithium-ion batteries. *Energy Environ. Sci.* **2023**, *16*, 3564–3575.
[33] *Thermo scientific avantage data system for XPS* [Online]. https://www.thermofisher.cn/cn/zh/home/materials-science/learning-center/periodic-table.html (accessed Feb 1, 2023).
[34] Zhang, C.; Lyu, R.; Lv, W.; Li, H.; Jiang, W.; Li, J.; Gu, S. C.; Zhou, G. M.; Huang, Z. J.; Zhang, Y. B. et al. A lightweight 3D Cu nanowire network with phosphidation gradient as current collector for high-density nucleation and stable deposition of lithium. *Adv. Mater.* **2019**, *31*, 1904991.
[35] Wu, H. L.; Wei, K. Y.; Tang, B. H.; Cui, Y. X.; Zhao, Y.; Xue, M. Z.; Li, C. L.; Cui, Y. H. A novel Li_3P-VP nanocomposite fabricated by pulsed laser deposition as anode material for high-capacity lithium ion batteries. *J. Electroanal. Chem.* **2019**, *841*, 21–25.
[36] Liang, X.; Li, X.; Xiang, Q. X.; Zhang, S. J.; Cao, Y.; Han, M. Y.; Zhang, Y. M.; Zhou, C. Y.; Xu, Y. H.; Mao, C. et al. Surficial oxidation of phosphorus for strengthening interface interaction and enhancing lithium-storage performance. *Nano Lett.* **2022**, *22*, 9335–9342.
[37] Jagger, B.; Pasta, M. Solid electrolyte interphases in lithium metal batteries. *Joule* **2023**, *7*, 2228–2244.
[38] Li, N. W.; Yin, Y. X.; Yang, C. P.; Guo, Y. G. An artificial solid electrolyte interphase layer for stable lithium metal anodes. *Adv. Mater.* **2015**, *28*, 1853–1858.
[39] Peng, K. Y.; Chen, Z. Y.; Zhao, X. Y.; Shi, K. Y.; Zhu, C. B.; Yan, X. B. Dual-conductive Li alloy composite anode constructed by a synergetic conversion–alloying reaction with $LiMgPO_4$. *Chem. Eng. J.* **2022**, *439*, 135705.
[40] Liu, Y. Y.; Lin, D. C.; Li, Y. Z.; Chen, G. X.; Pei, A.; Nix, O.; Li, Y. B.; Cui, Y. Solubility-mediated sustained release enabling nitrate additive in carbonate electrolytes for stable lithium metal anode. *Nat. Commun.* **2018**, *9*, 3656.
[41] Gao, Y.; Yan, Z. F.; Gray, J. L.; He, X.; Wang, D. W.; Chen, T. H.; Huang, Q. Q.; Li, Y. C.; Wang, H. Y.; Kim, S. H. et al. Polymer–inorganic solid–electrolyte interphase for stable lithium metal batteries under lean electrolyte conditions. *Nat. Mater.* **2019**, *18*, 384–389.
[42] Zhang, X. Q.; Chen, X.; Cheng, X. B.; Li, B. Q.; Shen, X.; Yan, C.; Huang, J. Q.; Zhang, Q. Highly stable lithium metal batteries enabled by regulating the solvation of lithium ions in nonaqueous electrolytes. *Angew. Chem., Int. Ed.* **2018**, *57*, 5301–5305.
[43] Park, J. B.; Choi, C.; Yu, S.; Chung, K. Y.; Kim, D. W. Porous lithiophilic Li-Si alloy-type interfacial framework via self-discharge mechanism for stable lithium metal anode with superior rate. *Adv. Energy Mater.* **2021**, *11*, 2101544.
[44] Ju, Z. J.; Xie, Q. F.; Sheng, O. W.; Wu, X. X.; Tan, Y. H.; Hong, M.; Tao, X. Y.; Liang, Z. Biomass-derived anion-anchoring nano-$CaCO_3$ coating for regulating ion transport on Li metal surface. *Nano Lett.* **2022**, *22*, 5473–5480.
[45] Xiao, J.; Li, Q. Y.; Bi, Y. J.; Cai, M.; Dunn, B.; Glossmann, T.; Liu, J.; Osaka, T.; Sugiura, R.; Wu, B. B. et al. Understanding and applying Coulombic efficiency in lithium metal batteries. *Nat. Energy* **2020**, *5*, 561–568.
[46] Adams, B. D.; Zheng, J. M.; Ren, X. D.; Xu, W.; Zhang, J. G. Accurate determination of Coulombic efficiency for lithium metal anodes and lithium metal batteries. *Adv. Energy Mater.* **2018**, *8*, 1702097.
[47] Zhang, H.; Eshetu, G. G.; Judez, X.; Li, C. M.; Rodriguez-Martínez, L. M.; Armand, M. Electrolyte additives for lithium metal anodes and rechargeable lithium metal batteries: Progress and perspectives. *Angew. Chem., Int. Ed.* **2018**, *57*, 15002–15027.